SLICE EMITTANCE OPTIMIZATION AT THE SwissFEL INJECTOR TEST FACILITY

Eduard Prat,* Masamitsu Aiba, Simona Bettoni, Bolko Beutner, Marc Guetg,
Rasmus Ischebeck, Sven Reiche, Thomas Schietinger
Paul Scherrer Institut, CH-5232 Villigen PSI, Switzerland

Abstract

Slice emittance measurements with uncompressed beams at the SwissFEL Injector Test Facility have demonstrated emittances for bunch charges between 10 pC and 200 pC well below the tight requirements of the SwissFEL planned at the Paul Scherrer Institute. We present the measurement methods, emittance tuning strategies and results of this effort.

INTRODUCTION

The SwissFEL facility planned at the Paul Scherrer Institute will produce coherent, bright, and short photon pulses covering a wavelength range down to 1 Å, requiring emittances between 0.18 and 0.43 mm mrad for bunch charges between 10 pC and 200 pC. To demonstrate the feasibility of our beam design a test facility of the injector section was built and has been operated since 2010.

The natural length scale along the bunch to analyze beam properties related to the FEL performance is the slippage length, which is in our case about 0.3 µm for a wavelength of 1 Å at 200 pC. Thus longitudinally resolved emittance studies, so called slice emittance measurements, are of great interest and are performed at various machines. Early studies employed slit absorbers in dispersive sections for energy-chirped beams. The typical longitudinal resolution of this approach is of the order picosecond [1]. With transverse deflecting RF-structures, as used at FLASH or LCLS, resolutions on the order of about 10 femtoseconds are possible [2, 3].

We present the methods used for our longitudinally resolved transverse phase-space measurements as well as the optimization techniques applied, followed by the final results.

THE SWISSFEL INJECTOR TEST FACILITY

For details of the SwissFEL Injector Test Facility we refer to [4]. Nominally electron bunches of charges between 10 pC and 200 pC are generated in a CTF3-type 2.6-cell standing-wave S-band RF photoinjector gun using a Ti:Sapphire laser. A longitudinal flat-top profile is approximated by pulse stacking 32 replica. The beam energy at the gun exit is 7.1 MeV. A solenoid close to the gun cavity is used for initial focusing (invariant envelope matching). Additional individually powered windings inside the gun solenoid allow for correction of normal- and skew-quadrupole components.

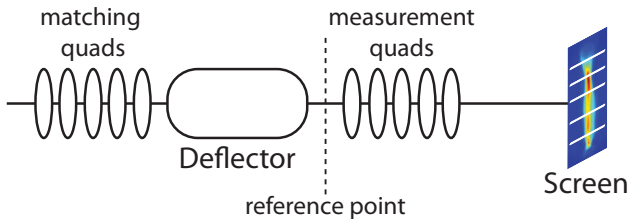

Figure 1: Schematic overview of the setup for slice emittance measurements at the SwissFEL Injector Test Facility.

Four S-band accelerating structures bring the beam energy up to the nominal value of 250 MeV. The structures are operated on-crest to maximize energy gain. Additional solenoid magnets around these structures allow for further control of the transverse optics. After some drift, which is to be used later for an X-band linearizing system and a bunch-compressor chicane, an S-band transverse deflecting cavity is used for longitudinally resolved measurements such as bunch length and slice emittance. The final beam energy is measured by a spectrometer at the beam dump.

SLICE EMITTANCE MEASUREMENTS

Moments of phase-space distributions can be determined by varying the betatronic beam transport between a reference point and a transverse beam profile monitor used for beam size measurements. Specifically we obtain the beam moments $\langle x_0^2 \rangle$, $\langle x_0'^2 \rangle$, and $\langle x_0 x_0' \rangle$ at the reference point from N measured beam sizes σ_i by using the corresponding transport functions R^i and solving the system of equations

$$\sigma_i^2 = {R_{11}^i}^2 \langle x_0^2 \rangle + {R_{12}^i}^2 \langle x_0'^2 \rangle + 2 R_{11}^i R_{12}^i \langle x_0 x_0' \rangle , \quad (1)$$

for $i \in 1, 2, ..., N$. From the measured beam moments the emittance and Twiss parameters can be derived. In principle three different transport functions are sufficient; in practice we use a much larger number of measurements and solve Eq. 1 by a least-square optimization (a detailed description of this procedure can be found in Ref. [5]). The quality and robustness of the measurement can be further increased by a proper choice of the transfer functions R^i, as described, e.g., in Ref. [6].

The above procedure is generic in the sense that it can also be used for slice-emittance measurements in combi-

* eduard.prat@psi.ch

ISBN 978-3-95450-126-7

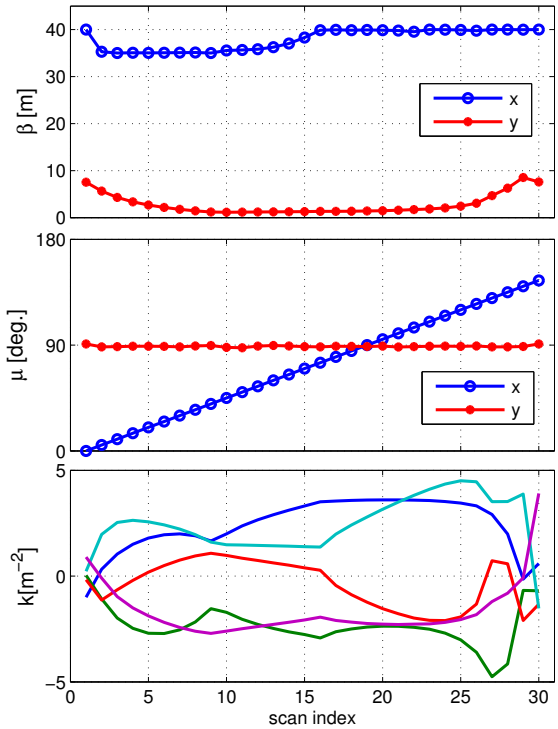

Figure 2: The β-functions at the measurement screen (top), phase advance between deflector and screen (middle), and the required k-values for the measurement quadrupoles during the scan (bottom), plotted for each scan index i. These values are only correct if the initial optics corresponds to the design optics.

nation with a transverse deflecting cavity, as indicated in Fig.1. Such a structure induces a transverse kick correlated with time on the bunch. After some drift this correlation gives rise to a transverse streak of the beam. The local beam size in the direction perpendicular to the streak, which is in the vertical plane at the SwissFEL Injector Test Facility, can be measured and utilized for emittance studies as described above.

Varying transport functions R^i are generated by a set of precalculated focusing strengths in a set of five quadrupoles [7, 3]. The optics setup used for our measurements is illustrated in Fig. 2. This set of optics transfer functions approximately respects certain boundary conditions: First the phase advance in the horizontal plane should cover as much of the $180°$ range as possible, while a constant phase advance fulfilling $\sin \mu_y = 1$ in the vertical plane, the streak direction, maximizes the observable correlation generated by the deflector. The β-function in the horizontal plane is optimized to have the expected beam sizes well within the dynamic range of our transverse profile monitor. In our case the horizontal β-function varies between 35 and 40 m. The optimized spot size will no longer be adequate if the emittance differs substantially from expectation. In such cases a new set of optics can easily be calculated.

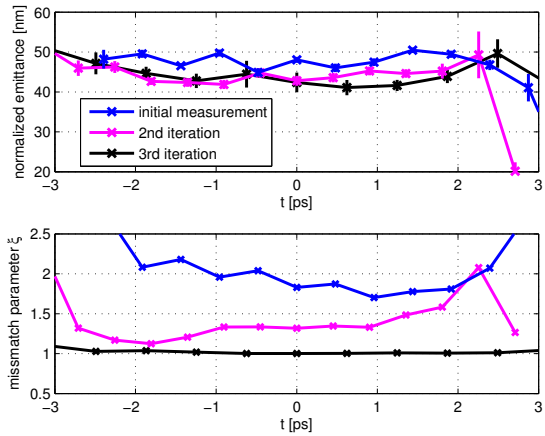

Figure 3: An example of matching iterations of the longitudinal beam core. The emittance measurements (top) are compared with the mismatch parameter ξ along the bunch (bottom). The beam charge is on the order of 1 pC.

The precalculated k-values, as shown in the bottom plot of Fig. 2, are only resulting in the desired optics if the initial optics (i.e. at the reference point) is matched to the design optics. Therefore it is mandatory to have the projected beam optics matched to these parameters. This is achieved by performing measurements as described in Ref. [6] using five upstream matching quadrupoles. The beam optics may, however, vary along the bunch and the projected beam optics may therefore differ from the optics at the longitudinal core of the bunch, which can result in distorted measurements. The longitudinally resolved beam-size measurements allow us to match the (horizontal) optics of *one individual slice* of the bunch to the design optics. As a typical example, Fig. 3 shows a comparison of matching iterations of the core slice optics. Similarly to the matching of the projected bunch we examine the reconstructed Twiss parameters of the beam core slice and compute corrections for a set of upstream matching quadrupoles to match the beam core to the design optics. Since the measurements can be compromised by the initial mismatch several iterations may be needed as illustrated in Fig. 3. As a general rule we consider measurements only to be reasonable if the local mismatch parameter, defined as $\xi = (\beta_0\gamma - 2\alpha_0\alpha + \gamma_0\beta)/2$ is close to unity. Typically we repeat both initial projected matching iterations as well as the core slice matching until mismatch parameters below 1.1 are reached, before we trust our measurements.

The quality of the beam-size measurements is critical for the emittance determination. Our primary transverse profile monitor consists of a scintillating screen made of YAG crystal. The screen setup is optimized for resolution through a proper choice of the observation angle, which mitigates effects arising from crystal thickness [8]. We estimated the spot size resolution experimentally by strongly focusing the beam on that screen. From this measurements

ISBN 978-3-95450-126-7

we estimate the beam-size resolution to be at most ≈15 µm, which is equivalent to an emittance resolution of ≈3 nm at a beam energy of 250 MeV and β_x = 35 m. The photon yield from the YAG crystal gives a good signal-to-noise ratio for bunch charges down to about 1 pC.

The longitudinal resolution is determined by the streak voltage and the R_{34} between the deflector and the screen. With the phase advance optimized to $\sin\mu_y \approx 1$, and a value of the β_y-function of 40 m at the deflector we obtain a longitudinal resolution of about 4 µm, corresponding to about 10 fs. This resolution is reached for the maximum voltage of 5 MV (corresponding to 5 MW power) in the deflecting structure and assuming ε_y = 0.5 µm and a beam energy of 250 MeV.

In our measurements, the streak factor is determined individually for each measurement (scan step) by analyzing the slope between deflector RF phase and vertical centroid position on the screen.

SLICE BEAM SIZE DETERMINATION

To obtain the longitudinally resolved horizontal beam sizes we have to divide our beam image into appropriate bands, so-called slices. Particular attention must be given to the requirement that a set of beam-size measurements σ_i for a given scan index i refer to the same physical longitudinal slice along the bunch, as shot-to-shot variations of beam arrival time, deflector RF phase or beam position may affect the position of slices on the screen. This is ensured by identifying a reference point in each image and map the slices with respect to this origin. In practice we determine the longitudinal centroid position of the bunch individually for each image by means of a Gauss fit. This is possible since in our case the beams typically have a smooth and relatively symmetric longitudinal profile. For irregular beam profiles as in Ref. [3] more advanced techniques are required. The transverse beam sizes σ_i of slices are also determined from Gauss fits to the respective horizontal profiles within the slices. An example is shown in Fig. 4.

MEASUREMENT ERRORS

The statistical errors on the measured emittance reported here are obtained by propagating statistical beam-size errors according to Eq. 1. For example a 5% beam-size measurement error results in a 2.7% emittance error if the phase advance $\Delta\mu_x$ per step i is 10°.

The systematic errors are of the same order of magnitude as the statistical ones. Contributions from the camera pixel size calibration and the imaging optics resolution are estimated to be on the order of 1 to 2%. Since the beam sizes are determined by Gauss fits, any deviation of the beam profiles from a Gaussian shape can give rise to a systematic offset. For our almost Gaussian beam profiles this effect is small and again estimated to be at the percent level.

Beam energy and quadrupole field errors modify the R^i transfer functions, leading to differences between the real beam transport and the fit to Eq. 1. As described above

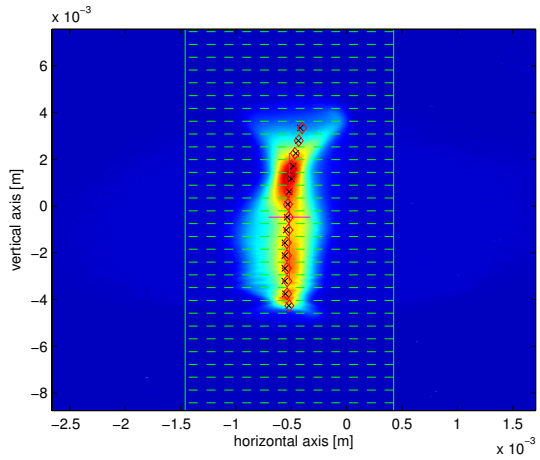

Figure 4: A typical image at the transverse profile monitor. The streak correlates the vertical with the longitudinal direction. Around the centroid (magenta cross) a region-of-interest is defined (green box), which is further divided into slices (dashed green lines). Centroid positions within each slice are calculated (red diamonds) and compared with the center of a Gaussian fit (black crosses).

we match the beam to the design optics such that possible error contributions from an optics mismatch are minimized. The remaining contribution to the error is estimated to be below 1%. The fact that the matching iterations converge quickly, as shown in Fig. 3, gives us additional confidence in our results. Any significant errors in the determination of beam moments would result in a much worse convergence behavior, and we would not attain consistently a mismatch of $\xi = 1$ for the beam core.

EMITTANCE OPTIMIZATION AND RESULTS

Efforts to minimize the emittance naturally fall into two categories: optimization of the electron source and mitigation of downstream emittance dilution effects.

At the source the performance of the laser system, in particular the transverse size and homogeneity of the laser spot on the cathode, are essential for reaching low emittance. On the accelerator side the setup of the gun RF cavity is of crucial importance. The effective energy gain as well as the relative phase between laser arrival time and gun RF need to be tuned while observing the beam in a dipole spectrometer. After the setup of the longitudinal dynamics in the gun we adjust the gun main solenoid focusing to the beam charge and energy so as to minimize the emittance. Residual quadrupole components in the gun solenoid are compensated by skew and normal quadrupole correctors integrated into the main solenoid. One objective of this initial beam tuning is the observation of symmetric beam spot at a screen upstream of the first symmetry-breaking quadrupole. For more details on the beam dynamics in the electron gun we refer to [4].

ISBN 978-3-95450-126-7

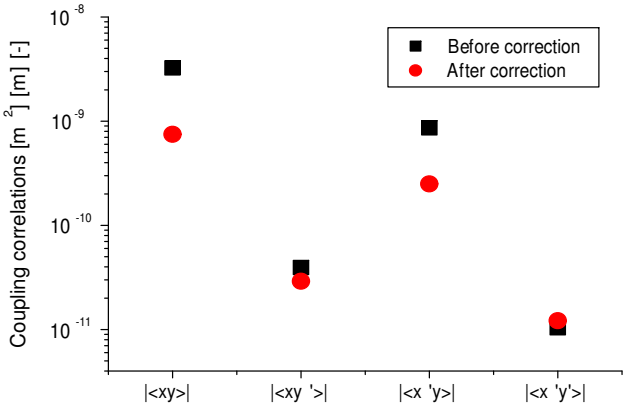

Figure 5: Coupling terms in the beam at different levels of correction.

For uncompressed beams (our measurements presented here) emittance degrading effects in the downstream beamline are dominated by off-axis RF fields and wake fields in the S-band booster structures. (In the case of compressed beams additional effects arise from coherent synchrotron radiation and longitudinal space charge.) An effective handle to control emittance dilution in the S-band booster is the beam orbit. We employ an orbit feedback to maintain a stable orbit in the RF structures. The emittance is then minimized by varying virtual offsets of the beam position monitors used as inputs in the feedback loop.

Coupling between the x-, and y-planes increases the emittance, unless the intrinsic emittance in an appropriately rotated coordinate system is measured. Our approach to minimize coupling consists in measuring and correcting coupling contributions with the gun corrector quadrupoles and four solenoids around the booster linac. The correlation coefficients $\vec{P} = \{\langle xy\rangle, \langle xy'\rangle, \langle x'y\rangle, \langle x'y'\rangle\}$ are measured using an expanded version of the system of equations (1), as described in [9]. Corrections are computed according to

$$\vec{C} = S^{-1} \cdot \vec{P}, \qquad (2)$$

where $\vec{C}$ represents possible corrections from available knobs and S^{-1} is the inverse of the so-called sensitivity matrix. The sensitivity matrix S relates an excitation of the correction knobs to the corresponding change in the coupling correlations. Using the corrections $\vec{C}$ the coupling terms can be reduced significantly, as shown in Fig. 5.

Our emittance measurements based on Eq. 1 does not include effects from dispersion. We therefore have to ensure that dispersion is not affecting the beam-size measurement at the screen location. It is, however, not straightforward to measure and remove all $R_{n,6}$ elements between any point in the machine and the measurement screen. A simple but effective method to avoid such complications is to generate local orbit bumps at the screen until the observed emittance is minimized. This effectively compensates any dispersion contributions from the upstream beamline, such that dispersion contributions to the emittance measurement are minimized. A summary of the various optimization techniques is given in Table 1.

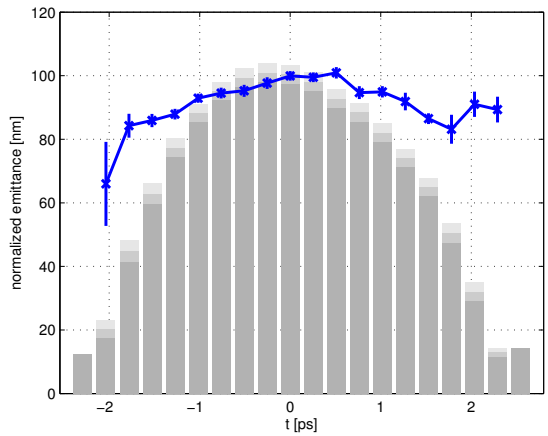

Figure 6: Normalized slice emittance in the horizontal plane for a bunch charge of 10 pC (blue). The error bars are obtained by error propagation of the statistical beam-size errors. For comparison the longitudinal bunch profile is shown as gray bars, with statistical errors indicated by different shading.

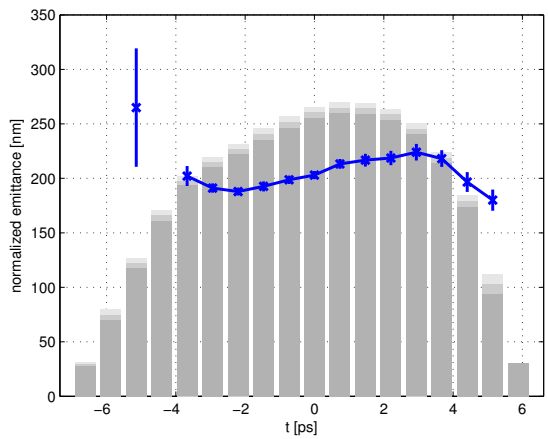

Figure 7: Same as Fig. 6 for a bunch charge of 200 pC.

The results of our slice emittance optimization, for SwissFEL standard operation modes, are summarized in Table 2 and shown graphically in Figs. 6 and 7 for 10 pC and 200 pC bunch charge, respectively. We achieved core slice emittances of $\varepsilon_x = 98 \pm 2$ nm rad for the 10 pC mode and $\varepsilon_x = 203 \pm 4$ nm rad for the 200 pC mode.

The excellent performance of our transverse profile monitor setup allows us to study bunch charges lower than 10 pC, which is the lowest design charge for SwissFEL operation. We were able to resolve slice emittance in bunches with charge down to about 1.5 pC. The lowest observed slice emittance in this charge range is $\varepsilon_x = 31.6 \pm 0.3$ nm rad (see Fig. 8).

ISBN 978-3-95450-126-7

Table 1: A Summary of "knobs" Used for Emittance Optimization in Order of the Electron Trajectory

knob	physics effect	comment
laser spot size on cathode	invariant envelope matching	iris set according to simulated optimum
transverse laser profile	emittance x/y symmetry	tuned to maximum homogeneity and symmetry
longitudinal laser profile	beam dynamics in the gun	tuned to flat top (lower emittance)
laser alignment	orbit, dispersion	standard beam-based alignment
gun phase	minimization of energy spread	minimization of horizontal beam size in spectrometer
gun gradient	invariant envelope matching	set to design energy using spectrometer (7.1 MeV)
gun solenoid alignment	orbit, dispersion	standard beam-based alignment
gun solenoid field	invariant envelope matching	emittance-based optimization
corrector quads	x/y coupling	empirical and systematic tuning
orbit in S-band booster	wake- and off-axis RF fields	emittance-driven beam-based alignment
orbit after S-band booster	dispersion at screen	beam-based alignment and local orbit bump

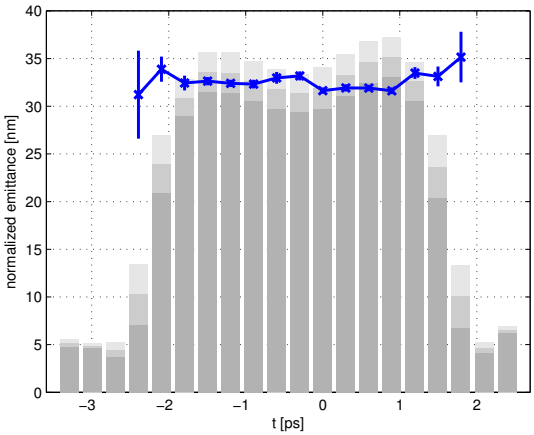

Figure 8: Same as Fig. 6 for a bunch charge of about 1.5 pC.

Table 2: Lowest Measured Core Slice and Projected Emittances for Different Bunch Charges. Errors are statistical (see text for details).

Q [pC]	$\varepsilon_{n,x}^{\text{slice}}$	$\varepsilon_{n,x}^{\text{proj}}$ [nm rad]	$\varepsilon_{n,y}^{\text{proj}}$
≈200	203±4	280±3	324±4
≈10	98±2	116±1	162±1
≈1.5	31.6±0.3	-	-

SUMMARY AND OUTLOOK

Measurements carried out at the SwissFEL Injector Test Facility with uncompressed beams have demonstrated slice emittances at the bunch core well suitable for SwissFEL operation and consistent with simulations. Current efforts at the test facility are focused on emittance studies with compressed beams, using a magnetic compression chicane in combination with an X-band phase-space linearizing system, and will be presented at a future opportunity.

ACKNOWLEDGMENTS

It is a pleasure to acknowledge the many contributions by the various PSI expert groups and the SwissFEL team to the construction and operation of the SwissFEL Injector Test Facility.

REFERENCES

[1] I. Ben-Zvi, J. X. Qiu and X. Wang, in Proceedings of the 17th Particle Accelerator Conference (PAC), Vancouver, Canada, 1997.

[2] P. Emma, J. Frisch, P. Krejcik, LCC-0047, LCLS-TN-00-12 (2000).

[3] M. Röhrs, PhD Thesis, DESY-THESIS-2008-012 (2008).

[4] M. Pedrozzi (ed.), "250 MeV Injector Conceptual Design Report", PSI Report 10-05 (2010).

[5] F. Löhl, Diploma Thesis, DESY-THESIS 2005-014, TESLA-FEL 2005-03 (2005).

[6] B. Beutner, E. Prat, in Proceedings of the 33rd International Free Electron Laser Conference (FEL), Shanghai, China, 2011.

[7] P. Tenenbaum, CLIC-Note-326 (1997).

[8] R. Ischebeck, to be published.

[9] E. Prat, M. Aiba, "4D Transverse Beam Matrix Measurement Using the Multiple-Quadrupole Scan Technique", to be published.

ISBN 978-3-95450-126-7